Materials Advances

ROYAL SOCIETY OF CHEMISTRY

PAPER

View Article Online
View Journal | View Issue

Cite this: *Mater. Adv.*, 2020, **1**, 2831

Development of an ultra-sensitive *para*-nitrophenol sensor using tri-metallic oxide $MoO_2{\cdot}Fe_3O_4{\cdot}CuO$ nanocomposites†

Md Abdus Subhan, *[a] Pallab Chandra Saha, [a] Jahir Ahmed,[a] Abdullah M. Asiri, [b] Mohammad Al-Mamun [c] and Mohammed M. Rahman *[b]

Received 21st August 2020,
Accepted 21st September 2020

DOI: 10.1039/d0ma00629g

rsc.li/materials-advances

A tri-metal oxide, $MoO_2{\cdot}Fe_3O_4{\cdot}CuO$ (TMO), was synthesized by the co-precipitation method and characterized by XRD, SEM-EDS, and FTIR. The average particle size of the nanocomposite was found to be 34.85 nm. The zeta potential and hydrodynamic size of the $MoO_2{\cdot}Fe_3O_4{\cdot}CuO$ nanocomposite were studied in acidic and basic pH respectively. A glassy carbon electrode (GCE) was modified by $MoO_2{\cdot}Fe_3O_4{\cdot}CuO$ to develop a chemical sensor for *para*-nitrophenol (*p*-NP). A simple I–V method was employed for this study. Excellent sensitivity, an ultra-low detection limit, long-term stability, and reproducibility of the $MoO_2{\cdot}Fe_3O_4{\cdot}CuO$/Nafion/GCE sensor were observed towards *p*-NP. A linear calibration plot (r^2: 0.9995) was obtained for 1.0 pM to 0.01 mM aqueous *p*-NP solution, with a sensitivity value of 5.2430 μA μM^{-1} cm^{-2} and remarkably low detection limit (LOD) of 0.2 pM.

Introduction

There have been a number of studies on advances of mixed metal oxide catalysts.[1–3] The electronic and molecular structures of metal oxides have attracted special attention because of the presence of multiple oxidation states and variable nonconventional local coordination. They have simultaneous bulk and surface phases as well as different surface functionalities. Mixed metal oxides comprise the largest family of heterogeneous catalysts for numerous applications. Composite oxides are better in terms of their catalytic activity than constituent oxides. It is due to the increasing active acidic or basic sites as well as the increasing surface area on mixed metal oxides.[4]

Many industrially important processes have been explored with mixed metal oxide nanocomposites.[5–7] Significant progress for technological development might be achieved by the use of those nano mixed metal oxides. MoO_2 is a larger bandgap semiconductor (3.85 eV) than MoO_3 (2.90 eV). When crystallized, MoO_2 showed spherical morphology whereas MoO_3 forms hexagonal or rectangular plates, based on the synthesis conditions.[8,9] MoO_2 has excellent applications in field emission devices, promising anode materials, and optical materials.[9] Thermodynamically, the stability of the amorphous phases is lower than that of orthorhombic MoO_3.[10] This oxide is normally found in the orthorhombic phase, which has many applications. This phase can be described as a layered structure formed by covalent double layers of MoO_6 octahedra. There have been studies on the antimicrobial, antioxidant, and cytotoxic effects of molybdenum oxide nanoparticles.[11]

In nature, iron(III) oxide is found in the form of rust. Generally, iron oxides are widespread, widely used as they are inexpensive, and play an important role in many biological as well as geological processes. They are also extensively used by humans including iron ores in thermite, catalysts, durable pigments (coatings, paints, and colored concrete), and hemoglobin. The three most common forms of iron oxides in nature are magnetite (Fe_3O_4), maghemite (γ-Fe_2O_3), and hematite (α-Fe_2O_3). NPs composed of ferromagnetic materials and with size $<$10–20 nm exhibit a unique form of magnetism, *i.e.*, super *para*-magnetism.

Oxide-based nanomaterials such as CuO have been gaining interest in nanomaterials research. Semiconducting oxides such as CuO and Cu_2O have distinguishing properties and are now widely used as transparent semiconducting oxide materials and chemical and biological sensors. This study was conducted to synthesize and characterize a tri-metal oxide from single metal oxides of interest, for exploring electrochemical

---

[a] *Department of Chemistry, School of Physical Sciences, Shahjalal University of Science and Technology, Sylhet-3114, Bangladesh. E-mail: subhan-che@sust.edu; Tel: +8801716073270*

[b] *Center of Excellence for Advanced Materials Research (CEAMR) & Department of Chemistry, Faculty of Science, King Abdulaziz University, P.O. Box 80203, Jeddah 21589, Saudi Arabia. E-mail: mmrahman@kau.edu.sa, mmrahmanh@gmail.com; Fax: +966-12-695-2292; Tel: +966-59-642-1830*

[c] *Centre for Clean Environment and Energy, Griffith School of Environment, Gold Coast Campus, Griffith University, QLD 4222, Australia*

† Electronic supplementary information (ESI) available. See DOI: 10.1039/d0ma00629g

sensor applications, because trimetallic oxide nanocomposites are promising systems for toxin sensors, photocatalytic applications and environmental safety, an efficient anti-bacterial agent against MDR bacteria, and industrial sterilization mediators.[12–16]

Phenolic compounds and their derivatives are extensively used in the production of pharmaceuticals, dyes, pesticides, *etc.*, and are known as severe environmental toxins.[17,18] They cause severe damage to organisms and plants.[19] *para*-Nitrophenol (*p*-NP) is an ingredient of the parathion-insecticide, which is a reason for anxiety because of its severe effects. *p*-NP is considered as one of the major toxic pollutants by the US Environmental Protection Agency (EPA).[20,21] As a result, for ecological security and food safety, there is an urgent need to produce an effective method for the detection and quantification of *p*-NP. Some traditional analytical methods have been reported for the detection of *p*-NP.[22–25] The electrochemical method offers various potential advantages such as a fast response, cost-effectiveness, and simple operation steps with good sensitivity and selectivity for the detection of *p*-NP. Electrodes including gold and glassy carbon electrodes in the electrochemical analysis are known to show good performance. However, still there is a need for ultrasensitive detection for a very low concentration of *p*-NP in pM in water. Modification of electrodes with various nanostructured materials may offer such opportunities.[26,27] Carbon-based nanomaterial containing electrodes such as carbon paste, carbon nanotube, and graphene electrodes are used extensively in the electrochemical determination of *p*-NP.[28,29] Nanographene is an excellent electrode material for *p*-NP determination because of its excellent charge transport properties, large surface to volume ratio, high electrocatalytic activity, and thermal conductivity.[30,31] There have been studies on the detection of *p*-NP using graphene/graphene oxide modified electrodes within the range of a few hundred nanomolar.[32]

In the present study, we prepared a $MoO_2{\cdot}Fe_3O_4{\cdot}CuO$ nanocomposite by the co-precipitation method for the electrochemical detection of *p*-NP at ambient conditions. The structural and morphological properties of $MoO_2{\cdot}Fe_3O_4{\cdot}CuO$ were studied by various techniques. After synthesis of $MoO_2{\cdot}Fe_3O_4{\cdot}CuO$, we coated the nanocomposite onto a GCE for the evaluation of the electrochemical performance for the detection of *p*-NP.[33,34] Besides, we also compared the electrochemical response of the $MoO_2{\cdot}Fe_3O_4{\cdot}CuO$ nanocomposite with a bare GCE and $MoO_2{\cdot}Fe_3O_4{\cdot}CuO$/GCE for the detection of *p*-NP, which indicates that the $MoO_2{\cdot}Fe_3O_4{\cdot}CuO$ nanocomposite shows better performance.

Experimental section

Materials and methods

$MoCl_2$ (Sigma Aldrich, Germany), $Fe(NO_3)_3{\cdot}9H_2O$ (MERCK, India), $CuCl_2{\cdot}3H_2O$ (AR, BDH), Na_2CO_3 (AR, BDH), NaOH (AR, BDH), and HCl (AR, BDH) (GPR, BDH) were purchased and used without further purification. Disodium phosphate, monosodium phosphate, 2-aminophenol, 4-methoxyphenol, *p*-NP, 3-chlorophenol, 2,4-dinitrophenol, bisphenol A, hydrazine, paracetamol, 4-nitrophenyl hydrazine, and 5% ethanolic Nafion solution were also purchased from Sigma-Aldrich. All chemicals were of analytical grade and used without further purification. The identification of the crystal phase and evaluation of other structural information of the nanomaterials studied in this work was performed by X-ray diffraction (XRD, Bruker D8 Advance diffractometer, equipped with a graphite monochromator). The diffraction patterns were recorded within the 2θ angle range from 10° to 80° in the step scan mode at 0.05 steps and at a rate of 10 s per step.[34] The surface morphology was studied using a Scanning Electron Microscope (SEM) with an Energy-Dispersive X-ray Spectrometer (EDS) (JSM-7100F) linked with an EDS mapping appliance. FTIR analysis of the samples was carried out using an FTIR spectrometer (Shimadzu, FTIR-8400S). The hydrodynamic size and zeta potential were measured using a Zetasizer Nanoseries (Nano-ZS90). *I–V* measurements of the fabricated $MoO_2{\cdot}Fe_3O_4{\cdot}CuO$/Nafion/GCE composites were conducted to detect *p*-nitrophenol using a Keithley electrometer (6517A, USA) at ambient conditions as reported recently.[34]

Preparation of the TMO $MoO_2{\cdot}Fe_3O_4{\cdot}CuO$ nanocomposite

The $MoO_2{\cdot}Fe_3O_4{\cdot}CuO$ nanocomposite was synthesized by a reliable and low-cost co-precipitation method. This synthetic process was started by preparing 0.25 M solutions of $MoCl_2$, $Fe(NO_3)_3{\cdot}9H_2O$, and $CuCl_2{\cdot}3H_2O$, which act as sources of molybdenum, iron, and copper, respectively. All of them were mixed in a beaker in the same volume ratio (50 mL) with constant stirring for 15 minutes. To the above mixture 0.5 M Na_2CO_3 was added dropwise until completion of the reaction at 45 °C. The resultant mixture was stirred constantly for another 1 hour at 45 °C. When the reaction was completed, the white precipitate was separated from the solution by centrifugation, then washed several times with deionized water and finally dried at 120 °C in an oven for 2 hours. The white sample was calcined in an electric muffle furnace (Gallenkamp, Korea) at 600 °C.[35] The calcination transformed the metal carbonates into metal oxides.[36] The reactions can be summarized as below:

$$(Mo^{2+} + Cl^-) + (Na^+ + CO_3^{\ 2-}) + HOH \rightarrow MoCO_3{\cdot}(OH)_2 + CO_2 + (Na^+ + Cl^-)$$

$$2Fe(NO_3)_3{\cdot}9H_2O + 3(Na^+ + CO_3^{\ 2-}) + HOH \rightarrow Fe_2(CO_3)_2{\cdot}(OH)_2 + (Na^+ + NO_3^{\ -})$$

$$(Cu^{2+} + Cl^-) + (Na^+ + CO_3^{\ 2-}) + HOH \rightarrow CuCO_3{\cdot}(OH)_2 + (Na^+ + Cl^-)$$

$$3MoCO_3{\cdot}(OH)_2 \rightarrow 3MoO_2 + 3CO_2$$

$$3Fe_2(CO_3)_2{\cdot}(OH)_2 \rightarrow 2Fe_3O_4 + 6CO_2$$

$$CuCO_3{\cdot}(OH)_2 \rightarrow CuO + CO_2$$

$$MoO_2 + Fe_3O_4 + CuO \rightarrow MoO_2{\cdot}Fe_3O_4{\cdot}CuO$$

Modification of a GCE with the TMO nanocomposite

The synthesized $MoO_2{\cdot}Fe_3O_4{\cdot}CuO$ was used to fabricate a GCE by using a 5% ethanolic solution of Nafion to get an approximately 0.4 mm thick film. It was then heated in an oven at 45.0 °C for 2 hours to get the dry film on the GC electrode. In an electro-chemical cell, the $MoO_2{\cdot}Fe_3O_4{\cdot}CuO$ nanocomposite fabricated GCE was used as a working electrode (WE), a platinum wire was the counter electrode (CE), and aqueous *p*-NP in 0.1 M phosphate buffer solution (PBS; pH 7.0) was used as the supporting electrolyte. To utilize the target chemical, aqueous *p*-NP (1.0 mM) was systematically diluted to various concentrations (1.0 mM to 1.0 pM) using deionized water. All the *I–V* measurements were performed in 5.0 mL of PBS (pH = 7.0). From the slope of the calibration plot, the sensitivity of the proposed *p*-NP sensor was calculated by considering the active surface area of the GCE. By using an electrometer (Keithley, 6517A electrometer, USA) the *I–V* method was applied to aqueous *p*-NP taking $MoO_2{\cdot}Fe_3O_4{\cdot}CuO$/GCE as a working electrode.

Results and discussion

Structural characterization of the $MoO_2{\cdot}Fe_3O_4{\cdot}CuO$ nanocomposite

The XRD pattern of $MoO_2{\cdot}Fe_3O_4{\cdot}CuO$ is as depicted in Fig. 1. There are three oxides MoO_2, Fe_3O_4 and CuO in the synthesized nanocomposite. One of them is monoclinic, $C2/c(15)$, tenorite (CuO), which shows peaks at 2θ = 32.505°, 35.498°, 38.698°, 46.153°, 48.702°, 51.346°, 58.144°, 61.548°, 65.659°, 66.152°, 67.954°, and 72.208° (JCPDS#72-0629) with lattice constants *a*, *b*, *c* and ($\alpha\beta\gamma$) of 4.6837, 3.4226, 5.1288 and (90.0 × 99.54 × 90.0), density (ρ) = 6.515 and volume = 81.1. Another one is magnetite (Fe_3O_4) (cubic, $Fd\bar{3}m(227)$) having 2θ = 18.326°, 35.498°, 37.139°, 43.01°, 57.044°, 66.152°, 71.101°, 74.243°, and 79.086° (JCPDS#88-0315). Its lattice constants *a*, *b*, *c* and ($\alpha\beta\gamma$) are 8.375, 8.375, 8.375 and (90.0 × 90.0 × 90.0) with density (ρ) = 5.235, and volume 587.4. The third one is also monoclinic, $P21/c(14)$, MoO_2, with 2θ peaks at 18.326°, 37.139°, 41.303°, 41.913°, 49.467°, 59.834°, 63.999°, 66.152°, 70.306°, 72.208°, and 79.086° (JCPDS#86-0135). Its lattice constants *a*, *b*, *c* and ($\alpha\beta\gamma$) are 5.609, 4.86, 5.628 and (90.0 × 120.94 × 90.0) respectively. The particle size of the nanocomposite was estimated from XRD data using Scherrer's formula $\tau = K\lambda/(\beta\cos\theta)$. Here τ is the mean size, K is a dimensionless shape factor with a value 0.94, λ is the X-ray wavelength (0.1506 nm), β is the line broadening at half the maximum intensity (FWHM) and θ is the Bragg angle. The average particle size of the $MoO_2{\cdot}Fe_3O_4{\cdot}CuO$ nanocomposite was found to be 34.85 nm.

Morphological and elemental analysis of the $MoO_2{\cdot}Fe_3O_4{\cdot}CuO$ nanocomposite

An SEM study (as in Fig. 2a and b) was performed to reveal a clear image of the surface morphology and particles of synthesized nanocomposite $MoO_2{\cdot}Fe_3O_4{\cdot}CuO$. Fig. 2(a) shows that the nanocomposite formed in mixed cubic, rectangular and spherical morphologies. EDS mapping was carried out to map the elemental compositions of the nanocomposite. As is seen from the EDS data (Fig. S1 and Table S1, ESI†) the nanocomposites consist of Mo, Fe, Cu, and O with an atomic percentage of 2.5%, 30.85%, 14.8%, and 51.85% respectively. The EDS mapping also indicated that the elements were distributed throughout the matrix (Fig. S2, ESI†).

FTIR study of the $MoO_2{\cdot}Fe_3O_4{\cdot}CuO$ nanocomposite

Fig. S3 (ESI†) shows the FTIR spectrum of the $MoO_2{\cdot}Fe_3O_4{\cdot}CuO$ nanocomposite in 400–4000 cm^{-1}. The band centred at 3433 cm^{-1} is assigned to the stretching mode of atmospheric H_2O.[37] The FTIR spectrum of the sample calcined at 600 °C showed the stretching mode of Mo=O at 966 cm^{-1} and Mo–O at 823 cm^{-1}, and 775 cm^{-1}. The IR peak at 717 cm^{-1} is attributed to the Mo–O–Mo stretching vibrations.[38] The sample exhibited an intense peak at 599 cm^{-1} due to the stretching vibration mode associated with the iron–oxygen band (Fe–O bonds in the crystalline lattice of Fe_3O_4).[39] The peak at 433 cm^{-1} is attributed to the

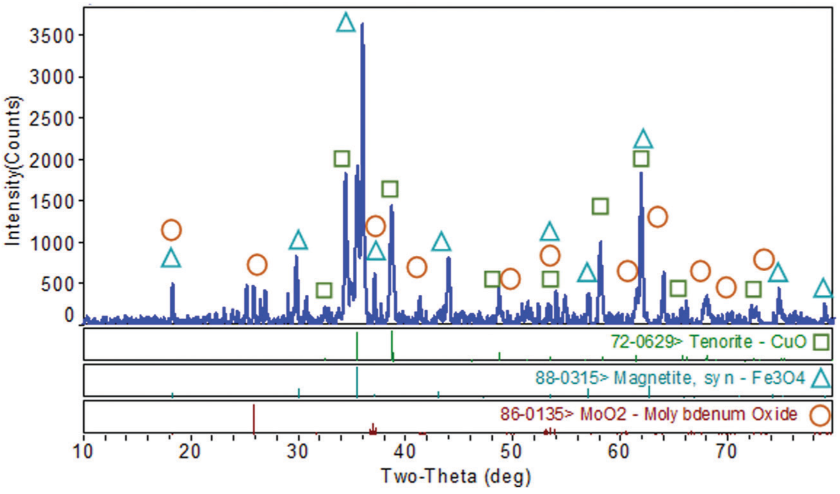

Fig. 1 XRD pattern of the $MoO_2{\cdot}Fe_3O_4{\cdot}CuO$ nanocomposite.

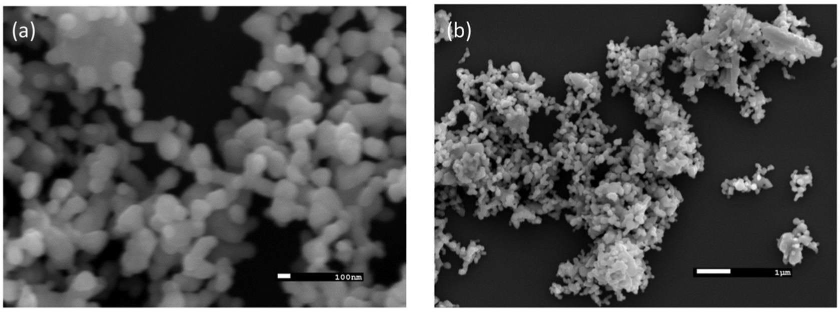

Fig. 2 SEM image of ternary $MoO_2{\cdot}Fe_3O_4{\cdot}CuO$ nanocomposites at different magnification (a and b).

Cu–O bond frequency. No peak at 873 cm^{-1} was found, which may indicate that there is no CO_3^{2-} left in $MoO_2{\cdot}Fe_3O_4{\cdot}CuO$. Thus, the nanocomposite contains only oxides with little or no unknown compounds.

Zeta potential and hydrodynamic size of the $MoO_2{\cdot}Fe_3O_4{\cdot}CuO$ nanocomposite

The zeta potential and hydrodynamic size of the $MoO_2{\cdot}Fe_3O_4{\cdot}CuO$ nanocomposite were studied in acidic and basic pH to know the size and charge in dispersed media. The hydrodynamic size, zeta potential, and polydispersity index (PDI) are listed in Table 1. The hydrodynamic size of $MoO_2{\cdot}Fe_3O_4{\cdot}CuO$ in acidic pH and basic pH was found to be 1284 and 850.7 nm. The zeta potential in acidic and basic pH has been observed to be −24.7 and −24.55 meV respectively. The results indicated that negatively charged $MoO_2{\cdot}Fe_3O_4{\cdot}CuO$ particles may adsorb organic compounds, dyes, and organic chemical toxins on the particle surface and perform catalytic functions.

Applications: chemical sensor study of the $MoO_2{\cdot}Fe_3O_4{\cdot}CuO$/Nafion/GCE assembly.

Detection of *p*-NP using $MoO_2{\cdot}Fe_3O_4{\cdot}CuO$/Nafion/GCE by the *I–V* method

Toxic *p*-NP in an aqueous system was determined using the $MoO_2{\cdot}Fe_3O_4{\cdot}CuO$ nanocomposite modified GC electrode. When *p*-NP comes into contact with $MoO_2{\cdot}Fe_3O_4{\cdot}CuO$, it produces a significant response in the *I–V* technique. The possible use of the *p*-NP sensor constructed from the $MoO_2{\cdot}Fe_3O_4{\cdot}CuO$/Nafion/GCE assembly was tested to detect and measure the selected toxin in phosphate buffer solution (PBS). The $MoO_2{\cdot}Fe_3O_4{\cdot}CuO$/Nafion/GCE sensor exhibits several advantages such as higher stability in air, improved electro-chemical properties during the determination, versatile operation, and safe electrochemical characteristics.[33,34] The probable application of the chemical sensor with $MoO_2{\cdot}Fe_3O_4{\cdot}CuO$/Nafion/GCE was evaluated in detail for the detection of selected compound *p*-NP in buffer solution and $MoO_2{\cdot}Fe_3O_4{\cdot}CuO$/Nafion/GCE acted as an electron mediator during the sensing process. The $MoO_2{\cdot}Fe_3O_4{\cdot}CuO$/Nafion/GCE assembly was tested as a working electrode for the construction of the proposed sensor for the targeted toxin *p*-NP. In the sensing procedure of *p*-NP in PBS solution, the applied current *vs.* potential (*I–V*) was examined on a thin film of $MoO_2{\cdot}Fe_3O_4{\cdot}CuO$/Nafion/GCE in the working electrode, which was increased noticeably due to the adsorption of aqueous *p*-NP on the fabricated working electrode. 1.0 sec was set as the holding period in the electrometer and an improved current *vs.* potential was detected in the time of *p*-NP determination by the fabricated chemical sensor.[35] A suggested oxidation mechanism of *p*-NP is demonstrated in Scheme 1. At the time of *p*-NP oxidation by the constructed working electrode with the $MoO_2{\cdot}Fe_3O_4{\cdot}CuO$/Nafion/GCE assembly, an enrichment of electrons in the buffer solution was detected and it caused an enhancement of the current *vs.* potential response during the *I–V* measurement at ambient conditions. According to the proposed *p*-NP oxidation mechanism, at the beginning, *p*-NP was converted to 4-hydroxylaminophenol, and, in the second step, 4-hydroxylaminophenol was oxidized to 4-nitrosophenol, followed by a consequent reversible reduction,[40] which are presented in eqn (i) and (ii).

$$\text{HO-Ph-NO}_2 + 4e^- + \text{H}^+ \rightarrow \text{HO-Ph-NHOH} + \text{H}_2\text{O} \tag{i}$$

$$\text{HO-Ph-NHOH} \leftrightarrow \text{HO-Ph-NO} + 2e^- + \text{H}^+ \tag{ii}$$

The pictorial application of the $MoO_2{\cdot}Fe_3O_4{\cdot}CuO$/Nafion/GCE modified electrode as a *p*-NP chemical sensor is demonstrated in Scheme 1.

A GCE was coated with a slurry of $MoO_2{\cdot}Fe_3O_4{\cdot}CuO$ nanomaterials. The constructed working electrode was applied for detection of *p*-NP compounds due to the oxidation in the buffer system which is proposed and presented above as per chemical reactions eqn (i) and (ii). According to the electrochemical oxidation process of targeted *p*-NP, several electrons were released to the conduction band, which enhanced the *I–V* response of the $MoO_2{\cdot}Fe_3O_4{\cdot}CuO$/Nafion/GCE sensors.

Fig. 3(a) shows the current responses for nine toxic chemicals, where (1.0 μM; 25.0 μL) *p*-NP solution (red line) in PBS (pH = 7.0)

Table 1 Hydrodynamic size and zeta potential of the $MoO_2{\cdot}Fe_3O_4{\cdot}CuO$ nanocomposite

	Na-citrate buffer (pH 4.95)			PBS buffer (pH 7.4)		
Compound	Size (nm)	Zeta potential	PDI	Size (nm)	Zeta potential	PDI
$MoO_2{\cdot}Fe_3O_4{\cdot}CuO$	1234	−24.55	0.66	850.7	−24.7	0.33

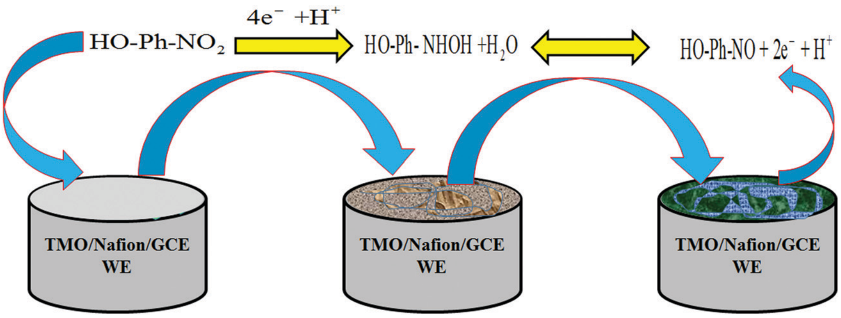

Scheme 1 The proposed mechanism in detection of *p*-NP by $MoO_2 \cdot Fe_3O_4 \cdot CuO$/Nafion/GCE.

produces a distinct peak at +0.3 V with the $MoO_2 \cdot Fe_3O_4 \cdot CuO$/Nafion/GCE surface. How the electrochemical property of $MoO_2 \cdot Fe_3O_4 \cdot CuO$ changes with the pH values was studied in PBS with pH values of 5.7 to 8.0 as in Fig. 3(b). The obtained results showed that $MoO_2 \cdot Fe_3O_4 \cdot CuO$ exhibits better electrochemical performance at different pH values. The electrocatalytic property of $MoO_2 \cdot Fe_3O_4 \cdot CuO$ changes with the pH values, which is revealed by the variation of the current response. In the pH optimization using *p*-NP (1.0 μM; 25.0 μL) in PBS, pH value 7.0 produces the maximum current response. Hence, pH value 7.0 was used in the rest of the experimental work in this *p*-NP determination by the $MoO_2 \cdot Fe_3O_4 \cdot CuO$/Nafion/GCE assembly. In the absence of target *p*-NP, the electrochemical signal intensities of the $MoO_2 \cdot Fe_3O_4 \cdot CuO$/GCE sensor probe at different pH values are measured and the signal is found to not significantly change in identical conditions (Fig. S4a, ESI†). The signal intensities of the $MoO_2 \cdot Fe_3O_4 \cdot CuO$/GCE sensor probe at different times (in the absence of *p*-NP) are also evaluated in identical conditions (Fig. S4b, ESI†). It is observed that no significant changes are found in the electrochemical response for elongated time in the absence of target analyte *p*-NP. The current intensities using *p*-NP (1.0 μM; 25.0 μL) in PBS (5.0 mL, pH = 7.0) for the bare GCE (blue line) and $MoO_2 \cdot Fe_3O_4 \cdot CuO$ fabricated GCE (red line) are given in Fig. 3(c). $MoO_2 \cdot Fe_3O_4 \cdot CuO$/Nafion/GCE produces a much better response than the bare GCE, which demonstrates the excellent electrochemical property of $MoO_2 \cdot Fe_3O_4 \cdot CuO$ as a selective *p*-NP sensor. Fig. 3(d) shows the current response of the $MoO_2 \cdot Fe_3O_4 \cdot CuO$ fabricated GCE in the absence of *p*-NP (blue line) and the presence of *p*-NP (red line; 1.0 μM; 25.0 μL) in 5.0 mL of PBS. With *p*-NP, a remarkable increase of the current response indicates the *p*-NP sensing capability of the proposed $MoO_2 \cdot Fe_3O_4 \cdot CuO$/Nafion/GCE sensor. The *I*–*t* response for *p*-NP (1.0 μM; 25.0 μL) in 5.0 mL of PBS solution using the $MoO_2 \cdot Fe_3O_4 \cdot CuO$ nanostructure fabricated

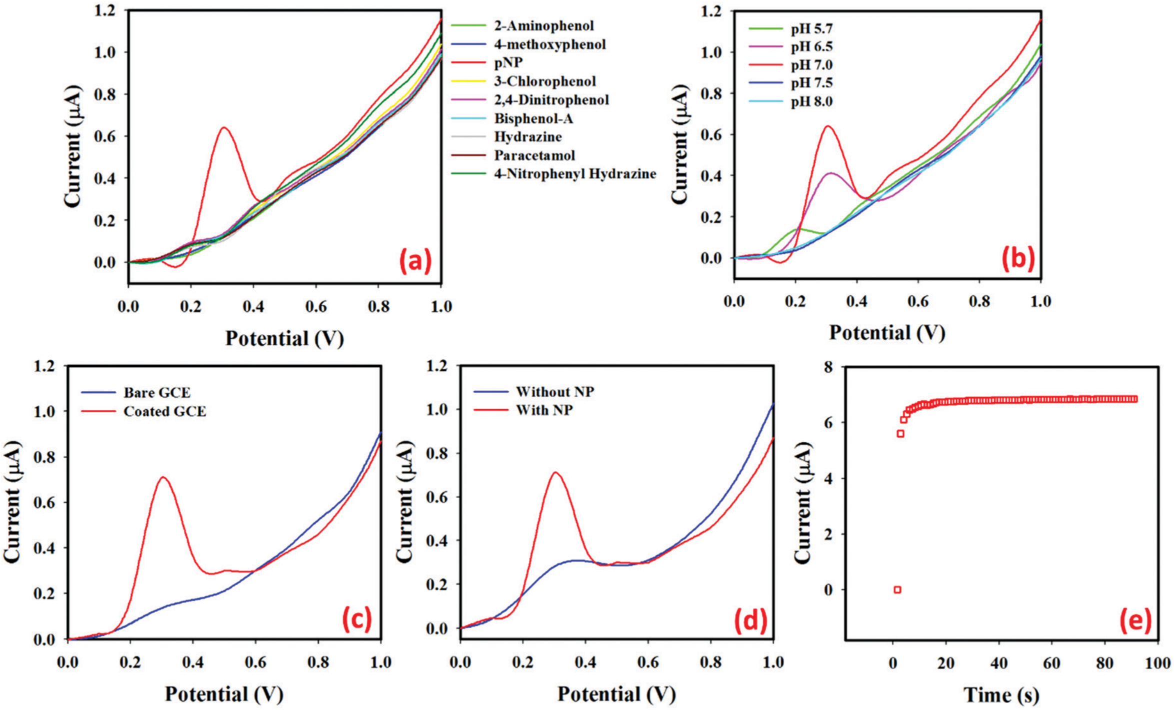

Fig. 3 *I*–*V* responses: (a) selectivity study using nine interferents, (b) pH variation; (c) bare GCE and $MoO_2 \cdot Fe_3O_4 \cdot CuO$/GCE, and (d) without and with the presence of *p*-NP (1.0 μM; 25.0 μL), and (e) current variation with time for $MoO_2 \cdot Fe_3O_4 \cdot CuO$/Nafion/GCE in 1.0 μM; 25.0 μL *p*-NP.

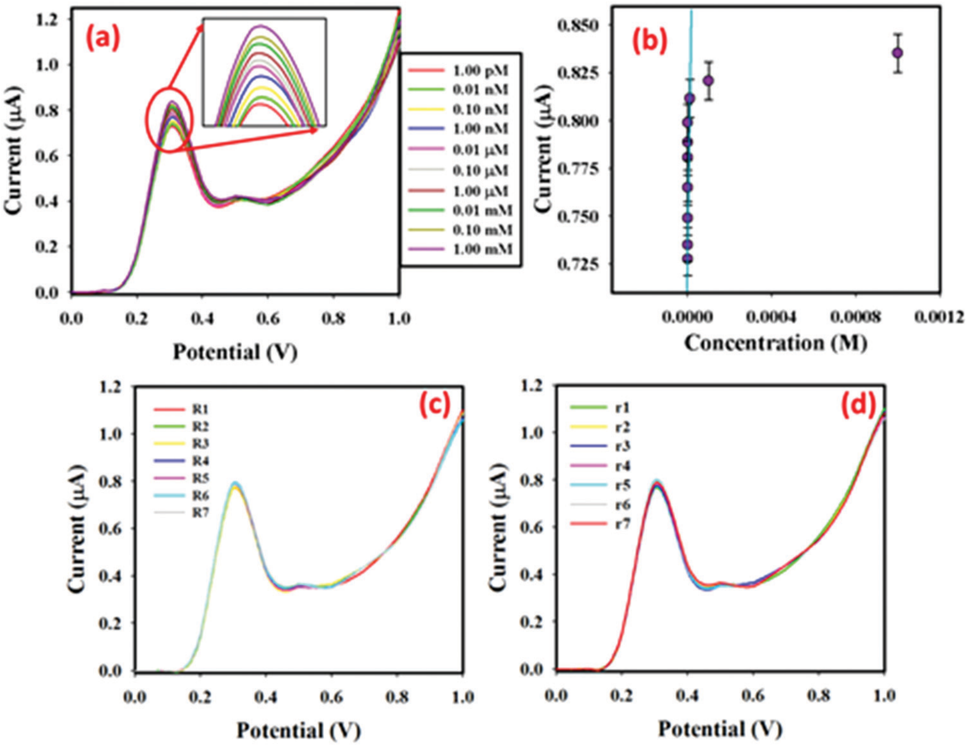

Fig. 4 (a) Current variations for different concentrations (1.0 pM to 1.0 mM) of aqueous *p*-NP in 0.0 to +1.0 V, (b) calibration plot of the $MoO_2 \cdot Fe_3O_4 \cdot CuO$ fabricated GCE at +0.3 V, (c) repeatability using different WEs (0.1 µM, 25.0 µL *p*-NP; 5.0 mL, 0.1 M PBS at pH 7.0), and (d) reproducibility using the same WE (0.1 µM, 25.0 µL *p*-NP; 5.0 mL, 0.1 M PBS at pH 7.0).

GCE as a working electrode is shown in Fig. 3(e). With *p*-NP (1.0 µM; 25.0 µL) in 5.0 mL of PBS, a constant current response was obtained in approximately 10 seconds. The *p*-NP chemical sensor is also optimized with various single metal oxides (*i.e.*; CuO, Fe_3O_4, and MoO_2) and compared with the $MoO_2 \cdot Fe_3O_4 \cdot CuO$ nanostructure in identical conditions (Fig. S4c, ESI†). The highest current is observed with the $MoO_2 \cdot Fe_3O_4 \cdot CuO$ nanostructure/GCE sensor probe compared to the only CuO, Fe_3O_4, and MoO_2 modified individual material.

In 5.0 mL PBS, low (1.0 pM) to high (1.0 mM) concentration *p*-NP solutions (25.0 µL) were injected sequentially and the surface current response variations were studied after every injection. The *I–V* responses from the $MoO_2 \cdot Fe_3O_4 \cdot CuO$ fabricated GCE surface were estimated using an aqueous *p*-NP solution of different concentrations (1.0 pM to 1.0 mM), given in Fig. 4(a) (the inset shows the magnification peak current at 0.3 V). It showed that when the potential increases, the *I–V* responses are also increased for the $MoO_2 \cdot Fe_3O_4 \cdot CuO$ fabricated GCE sensor. It was also observed that, from dilute (1.0 pM) to concentrated (1.0 mM) *p*-NP solution, the *I–V* responses also increased regularly. Aqueous *p*-NP (1.0 pM to 1.0 mM) was taken to select the limit of detection (LOD) of the developed sensor. The calibration plot (at +0.3 V) for the full concentration range is given in Fig. 4(b). A higher sensitivity value of 5.2430 $\mu A\ \mu M^{-1}\ cm^{-2}$ was estimated from the calibration plot. From the calibration plot, the linear dynamic range of the developed $MoO_2 \cdot Fe_3O_4 \cdot CuO$/GCE sensor was attained as 1.0 pM to 0.01 mM (r^2 = 0.9995), and the LOD was estimated as 0.2 pM [3 × noise (N)/slope (S)]. Fig. 4(c) shows the reproducibility of the current response with the $MoO_2 \cdot Fe_3O_4 \cdot CuO$ fabricated GCE with 25.0 µL of 0.1 µM *p*-NP using seven distinct working electrodes in run R1 to R7 under the same experimental conditions. The almost similar current responses in all seven experiments confirm the outstanding reproducibility of the sensor (RSD = 4.17%, *n* = 7). Fig. 4(d) presents the repeatability where the same working electrode was used in run R1–R7. The almost similar *I–V* responses in the seven repeated experiments demonstrate the outstanding repeatability of the sensor (RSD = 3.85%, *n* = 7). With the same working electrode in different solutions with the same conditions, the *I–V* response decreases

Table 2 Analysis of some environmental samples with $MoO_2 \cdot Fe_3O_4 \cdot CuO$/Nafion/GCE by the electrochemical process

Real sample	*p*-NP concentration[a] added	*p*-NP concentration[a] determined[b] by $MoO_2 \cdot Fe_3O_4 \cdot CuO$/Nafion/GCE	Recovery[b] (%)	RSD[c] (%) (*n* = 3)
S1	2.000 nM	2.102 nM	105.1	3.1
S1	2.000 µM	2.056 µM	102.8	2.9
S2	2.000 nM	2.036 nM	101.8	2.8
S2	2.000 µM	2.006 µM	100.3	3.4

S1 and S2: real water samples collected from an industrial effluent treatment plant and Safa drinking water bottle respectively, Jeddah, Saudi Arabia. [a] Mean of three repeated determinations (S/N = 3) with $MoO_2 \cdot Fe_3O_4 \cdot CuO$/Nafion/GCE. [b] Concentration of *p*-NP determined/concentration of *p*-NP taken. [c] The relative standard deviation value indicates the precision among three repeated determinations.

Table 3 Comparison of sensor analytical parameters of other nanostructure materials with the $MoO_2{\cdot}Fe_3O_4{\cdot}CuO$/Nafion/GCE sensor probe using the electrochemical method for the detection of *p*-NP

Sensor material	Method	LDR	LOD	Sensitivity	Ref.
ABPGH	LSV	20 nM to 8.0 μM and 8.0 μM to 0.1 mM	8.0 nM	2.717, 1.8117 $\mu A\ \mu M^{-1}$	41
BDAC	LSV	Up to 500 μM	0.16 μM	5.810 $\mu A\ \mu M^{-1}\ cm^{-2}$	42
Fe_3O_4/graphene	DPV	0.01 to 0.10 mM	0.004 mM	$8.067 \times 10^{-5}\ \mu A\ mM^{-1}$	43
TLISS	DPV	1.43–55.93 and 55.93–553.7 μM	1.09 μM	—	44
NiO–CeO_2	CV	1 to 20 μM	2.48 μM	3.68 $A\ \mu M^{-1}\ cm^{-2}$	45
$MoO_2{\cdot}Fe_3O_4{\cdot}CuO$	***I–V***	**1.0 pM to 0.01 mM**	**0.2 pM**	**5.2430 $\mu A\ \mu M^{-1}\ cm^{-2}$**	**This work**

TLISS = tremella-like indium silver sulfide modified GCE, ABPGH = acetylene blackpaste and graphene hybrid, BDAC = biomass derived activated carbons.

slightly. This may be because of the fall of the number of active sites in $MoO_2{\cdot}Fe_3O_4{\cdot}CuO$ after each run.

Real sample analysis by the $MoO_2{\cdot}Fe_3O_4{\cdot}CuO$/Nafion/GCE sensor

To confirm the functionality of the proposed sensor material $MoO_2{\cdot}Fe_3O_4{\cdot}CuO$, $MoO_2{\cdot}Fe_3O_4{\cdot}CuO$/Nafion/GCE had been employed to determine *p*-NP in industrial effluent water and drinking water from a plastic bottle after 7 days of sunlight irradiation kept inside a car (S2). For this, we use the standard addition method to verify the accuracy of the aqueous *p*-NP determination. 25.0 μL of aqueous *p*-NP of different concentrations and equal amounts of real samples were mixed and analyzed in PBS (5.0 mL, pH 7.0) with $MoO_2{\cdot}Fe_3O_4{\cdot}CuO$/GCE as a WE. Table 2 presents the obtained outcomes, which demonstrated that the $MoO_2{\cdot}Fe_3O_4{\cdot}CuO$/GCE modified sensor exhibited a quantitative (~100%) recovery of *p*-NP. So, we can conclude that the *I–V* method can be an appropriate and reliable technique in analyzing real samples using the $MoO_2{\cdot}Fe_3O_4{\cdot}CuO$/Nafion/GCE assembly.

The *I–V* responses in the *p*-NP measurements mostly depend on the size, porosity, and morphology of the nanomaterials. When the $MoO_2{\cdot}Fe_3O_4{\cdot}CuO$ surface comes into contact with the reducing *p*-NP, a surface-mediated oxidation reaction takes place. Oxidation of *p*-NP provides electrons to the $MoO_2{\cdot}Fe_3O_4{\cdot}CuO$ nanocomposite surface, which ultimately enhances the conductance of the $MoO_2{\cdot}Fe_3O_4{\cdot}CuO$/Nafion/GCE assembly. Consequently, when the potential increases, the *I–V* response also increases. The $MoO_2{\cdot}Fe_3O_4{\cdot}CuO$/Nafion/GCE sensor has also displayed consistency and stability. Overall, the proposed $MoO_2{\cdot}Fe_3O_4{\cdot}CuO$/Nafion/GCE sensor for *p*-NP detection showed better performance than others as shown in Table 3.[41–45]

Conclusions

$MoO_2{\cdot}Fe_3O_4{\cdot}CuO$ was synthesized by the coprecipitation method. $MoO_2{\cdot}Fe_3O_4{\cdot}CuO$ was characterized by several techniques including XRD, SEM-EDS, hydrodynamic size and zeta-potential analysis, and FTIR. The average particle size of the nanocomposite was determined to be 34.85 nm. The surface morphology of the composite was observed in the SEM study. The zeta potential of $MoO_2{\cdot}Fe_3O_4{\cdot}CuO$ in acidic and basic pH has been observed to be −24.7 and −24.55 meV respectively. A $MoO_2{\cdot}Fe_3O_4{\cdot}CuO$/Nafion/GCE electrode was successfully employed as a chemical sensor for the determination of aqueous *para*-nitrophenol. The fabricated *p*-NP chemical sensor based on $MoO_2{\cdot}Fe_3O_4{\cdot}CuO$ coated on a GCE showed a very efficient electron mediator property in the oxidation of *p*-NP in the PBS system. The proposed $MoO_2{\cdot}Fe_3O_4{\cdot}CuO$/Nafion/GCE sensor for *p*-NP exhibits a high sensitivity (5.2430 $\mu A\ nM^{-1}\ cm^{-2}$) and ultra-low LOD = 0.2 pM with an excellent linear response (r^2: 0.9995) for a wide range of concentrations in a short response time. It initiated a new route in developing an effective chemical sensor using nanostructured nanomaterials for a sustainable and safe environment.

Conflicts of interest

We declare that there is no conflict of interest.

Acknowledgements

Md Abdus Subhan acknowledges Fulbright USA for offering a Fulbright Visiting Scholar Award 2018–2019 for 9 months. MOE (Ministry of Education), Bangladesh, Grant (PS 14290) is gratefully acknowledged for support. Center of Excellence for Advanced Materials Research (CEAMR), King Abdulaziz University, Jeddah, Saudi Arabia, is highly acknowledged for the lab facilities and instrumental support.

References

1 J. F. Brazdil, Bulk metal oxides, in *Characterization of Catalytic Materials*, ed. I. E. Wachs, Butterworth-Heinemann, Boston, Massachusetts, 1992, pp. 47–68.
2 I. E. Wachs and K. Segawa, Supported metal oxides, in *Characterization of Catalytic Materials*, ed. I. E. Wachs, Butterworth-Heinemann, Boston, Massachusetts, 1992, pp. 69–88.
3 C. L. Thomas, *Catalytic Processes and Proven Catalysts*, Academic Press, New York, 1970.
4 S. J. Singh and R. V. Jayaram, *Tetrahedron Lett.*, 2008, **49**, 4249.
5 M. M. Rahman, A. Umar and K. Sawada, Development of amperometric glucose biosensor based on glucose oxidase co-immobilized with multi-walled carbon nanotubes at low potential, *Sens. Actuators, B*, 2009, **137**, 327.
6 D. I. Enache, J. K. Edwards, P. Landon, B. Solsona-Espriu, A. F. Carley, A. A. Herzing, M. Watanabe, C. J. Kiely, D. W. Knight and G. J. Hutchings, *Science*, 2006, **311**, 362.

7 X. Guo, H. Zhou, T. Fan and D. Zhang, Electrochemical detection of p-nitrophenol on surface imprinted gold with lamellar-ridge architecture, *Sens. Actuators, B*, 2015, **220**, 33–39.

8 Z. C. Xiang, Q. Zhang, Z. Zhang, X. J. Xu and Q. B. Wang, Preparation and photoelectric properties of semiconductor MoO_2 micro/nanospheres with wide bandgap, *Ceram. Int.*, 2015, **41**, 977–981.

9 R. J. Elliot, *Phys. Rev.*, 1957, **108**, 1384.

10 C. Julien, A. Khelfa, O. M. Hussain and J. A. Nazri, *J. Cryst. Growth*, 1995, **156**, 235.

11 A. Fakhri and P. Afshar Nejad, *J. Photochem. Photobiol., B*, 2016, **159**, 211.

12 M. A. Subhan, T. P. Rifat, P. C. Saha, M. M. Alam, A. M. Asiri, M. M. Rahman and J. Uddin, Enhanced visible light-mediated photocatalysis, antibacterial functions and fabrication of a 3-chlorophenol sensor based on ternary $Ag_2O{\cdot}SrO{\cdot}CaO$, *RSC Adv.*, 2020, **10**(19), 11274–11291.

13 M. A. Subhan, P. C. Saha, S. A. Sumon, J. Ahmed, A. M. Asiri, M. M. Rahman and Al-M Mamun, Enhanced photocatalytic activity and ultrasensitive benzaldehyde sensing performance of a $SnO_2{\cdot}ZnO{\cdot}TiO_2$ nanomaterial, *RSC Adv.*, 2018, **8**, 33048–33058.

14 M. A. Subhan, S. S. Jhuma, P. C. Saha, M. M. Alam, A. M. Asiri, M. Al- Mamun, S. A. Attia, T. H. Emon, A. K. Azad and M. M. Rahman, Efficient selective 4-aminophenol sensing and antibacterial activity of ternary $Ag_2O_3{\cdot}SnO_2{\cdot}Cr_2O_3$ nanoparticles, *New J. Chem.*, 2019, **43**, 10352.

15 M. A. Subhan, S. S. Jhuma, P. C. Saha, J. Ahmed, A. M. Asiri, T. P. Rifat, T. Raihan, A. K. Azad and M. M. Rahman, Photocatalysis, enhanced anti-bacterial performance and discerning thiourea sensing of $Ag_2O{\cdot}SnO_2{\cdot}TiO_2$ heterostructure, *J. Environ. Chem. Eng.*, 2020, **8**, 104051.

16 M. A. Subhan, P. C. Saha, M. M. Rahman, J. Ahmed, A. M. Asiri and M. A. Mamun, Fabrication of a 2,4-dinitrophenol sensor based on Fe_3O_4@Ag@Ni nanomaterials and studies on their antibacterial properties, *New J. Chem.*, 2018, **42**, 872.

17 X.-Q. Qiao, Z.-W. Zhang, F.-Y. Tian, D.-F. Hou, Z.-F. Tian, D. Li and Q. Zhang, Enhanced catalytic reduction of *p*-nitrophenol on ultrathin MoS_2 nanosheets decorated noble-metal nanoparticles, *Cryst. Growth Des.*, 2017, **17**(6), 3538–3547.

18 X.-Q. Qiao, Z.-W. Zhang, D.-F. Hou, D.-S. Li, Y. Liu, Y.-Q. Lan, J. Zhang, P. Feng and X. Bu, Tunable MoS_2/SnO_2 P–N Heterojunctions for an Efficient Trimethylamine Gas Sensor and 4-Nitrophenol Reduction Catalyst, *ACS Sustainable Chem. Eng.*, 2018, **6**, 12375–12384.

19 Z. Liu, J. Du, C. Qiu, L. Huang, H. Ma, D. Shen and Y. Ding, Electrochemical sensor for detection of *p*-nitrophenol based on nanoporous gold, *Electrochem. Commun.*, 2009, **11**, 1365–1368.

20 H. Yin, Y. Zhou, S. Ai, L. Cui and L. Zhu, Electrochemical determination of 2-nitrophenol in water samples using Mg–Al–SDS hydrotalcite-like clay modified glassy carbon electrode, *Electroanalysis*, 2010, **22**(10), 1136–1142.

21 X. Huang, N. Qiu and D. Yuan, Direct enrichment of phenols in lake and sea water by stir bar sorption extraction based on poly (vinylpyridine-ethylene dimethacrylate) monolithic material and liquid chromatographic analysis, *J. Chromatogr.*, 2008, **A1194**, 134–138.

22 X. Guo, Z. Wang and S. Zhou, The separation and determination of nitrophenol isomers by high-performance capillary zone electrophoresis, *Talanta*, 2004, **64**, 135–139.

23 A. Niazi and A. Yazdanipour, Spectrophotometric simultaneous determination of nitrophenol isomers by orthogonal signal correction and partial least squares, *J. Hazard. Mater.*, 2007, **146**, 421–427.

24 H. Yin, Y. Zhou, S. Ai, X. Liu, L. Zhu and L. Lu, Electrochemical oxidative determination of 4-nitrophenol based on a glassy carbon electrode modified with a hydroxyapatite nano powder, *Microchim. Acta*, 2010, **169**, 87–92.

25 K. Giribabu, R. Suresh, R. Manigandan, S. Munusamy, S. P. Kumar, S. Muthamizh and V. Narayanan, Nanomolar determination of 4-nitrophenol based on a poly(methylene blue)-modified glassy carbon electrode, *Analyst*, 2013, **138**, 5811–5818.

26 M. K. Alam, M. M. Rahman, M. Abbas, S. R. Torati, A. M. Asiri, D. Kim and C. G. Kim, Ultra-sensitive 2-nitrophenol detection based on reduced graphene oxide/ZnO nanocomposites, *J. Electroanal. Chem.*, 2017, **788**, 66–73.

27 H. Yin, Y. Zhou, S. Ai, Q. Ma, L. Zhu and L. Lu, Electrochemical oxidation determination and voltammetric behaviour of 4-nitrophenol based on Cu_2O nanoparticles modified glassy carbon electrode, *Int. J. Environ. Anal. Chem.*, 2012, **92**(6), 742–754.

28 Y. Tang, R. Huang, C. Liu, S. Yang, Z. Lu and S. Luo, Electrochemical detection of 4-nitrophenol based on a glassy carbon electrode modified with a reduced graphene oxide/Au nanoparticle composite, *Anal. Methods*, 2013, **5**, 5508–5514.

29 J. Li, D. Kuang, Y. Feng, F. Zhang, Z. Xu and M. Liu, A graphene oxide-based electrochemical sensor for sensitive determination of 4-nitrophenol, *J. Hazard. Mater.*, 2012, **201–202**, 250–259.

30 K. Chen, Z.-L. Zhang, Y.-M. Liang, W. Liu and A. Graphene-Based, Electrochemical Sensor for Rapid Determination of Phenols in Water, *Sensors*, 2013, **13**, 6204–6216.

31 A. Arvinte, M. Mahosenaho, M. Pinteala, A.-M. Sesay and V. Virtanen, Electrochemical oxidation of *p*-nitrophenol using graphene-modified electrodes, and a comparison to the performance of MWNT-based electrodes, *Microchim. Acta*, 2011, **174**, 337–343.

32 M. M. Rahman, M. M. Alam, A. M. Asiri and M. A. Islam, Fabrication of selective chemical sensor with ternary ZnO/SnO_2/Yb_2O_3 nanoparticles, *Talanta*, 2017, **170**, 215–223.

33 M. A. Subhan, P. C. Saha, M. M. Rahman, M. A. R. Akand, A. M. Asiri and M. Al-Mamun, Enhanced photocatalytic activity and chemical sensor development based on ternary $B_2O_3{\cdot}Zn_6Al_2O_9{\cdot}ZnO$ nanomaterials for environmental safety, *New J. Chem.*, 2017, **41**(15), 7220–7231.

34 M. A. Subhan, T. Ahmed, P. Sarker, T. T. Pakkanen, M. Suvantoc, M. Horimoto and H. Nakata, *J. Lumin.*, 2014, **148**, 98.

35 Md A. Subhan, M. R. Awal, T. Ahmed and M. Younus, *Acta Metall. Sin.*, 2014, **27**(2), 223–232.

36 H. H. Kung, *Stud. Surf. Sci. Catal.*, 1989, **45**, 1.

37 N. Dukstiene, D. Sinkeviciute and A. Guobiene, *Cent. Eur. J. Chem.*, 2012, **10**(4), 1106–1118.

38 G. Gundiah and C. N. R. Rao, *Solid State Sci.*, 2000, **2**, 877.

39 Y. Haldorai, K. Giribabu, S. K. Hwang, C. H. Kwak, Y. S. Huh and Y. K. Han, Facile synthesis of a-MnO_2nanorod/graphene nanocomposite paper electrodes using a 3D precursor for supercapacitors and sensing platform to detect 4-nitrophenol, *Electrochem. Acta.*, 2016, **222**, 717–727.

40 M. M. Rahman, S. B. Khan, A. M. Asiri and A. G. Al-Sehemi, Chemical sensor development based on polycrystalline gold electrode embedded low-dimensional Ag_2O nanoparticles, *Electrochem. Acta.*, 2013, **112**, 422–430.

41 Q. He, Y. Tian, Y. Wu, J. Liu, G. Li, P. Deng and D. Chen, Facile and Ultrasensitive Determination of 4-Nitrophenol Based on Acetylene Black Paste and Graphene Hybrid Electrode, *Nanomaterials*, 2019, **9**, 429.

42 R. Madhu, C. Karuppiah, S.-M. Chen, P. Veerakumar and S.-B. Liu, Electrochemical detection of 4-nitrophenol based on biomass derived activated carbons, *Anal. Methods*, 2014, **6**, 5274–5280.

43 M. Sarno and E. Ponticorvo, Fe_3O_4/Graphene Electrode for the Electrochemical Detection of 4-Nitrophenol, *Chem. Eng. Trans.*, 2020, **79**, 427.

44 P. Chen, Y. Shi, X. Li, T. Wang, M. Zhou, E. Tian, W. Wang, H. Jiang and H. Shu, Highly Effective Detection of 4-Nitrophenol by Tremella-like Indium Silver Sulfide Modified GCE, *Int. J. Electrochem. Sci.*, 2018, **13**, 6158–6168.

45 N. Ahmad, M. Alam and R. Wahab, Synthesis of NiO–CeO_2 nanocomposite for electrochemical sensing of perilous 4-nitrophenol, *J. Mater. Sci.: Mater. Electron.*, 2019, **30**, 17643–17653.